

Enhancement in Tribological and Mechanical Properties of Cemented Tungsten Carbide Substrates using CVD-diamond Coatings

K.A. Najar^a, N.A. Sheikh^a, M.A. Shah^b

^a Department of Mechanical Engineering, National Institute of Technology Srinagar 190006, India,

^b Department of Physics, National Institute of Technology Srinagar 190006, India.

Keywords:

CVD-diamond
Grain growth
Nanocrystalline/microcrystalline
Nanoindentation
Al₂O₃ ceramic ball
Friction Coefficient
Tribo-layer

ABSTRACT

An experimental investigation has been carried out to study the influence on the performance characteristics of a cutting tool material notably known as cemented tungsten carbide (WC-Co). A comparison has been documented between nanocrystalline diamond (NCD) and microcrystalline diamond (MCD) coatings deposited on two cemented tungsten carbide (WC-Co) substrates with the architectures of WC-Co/NCD and WC-Co/MCD, using hot filament chemical vapor deposition (HFCVD) technique. In the present work, the friction characteristics were studied using ball-on-disc type linear reciprocating micro-tribometer, under the application of 1–10 N normal loads, when sliding against smooth alumina (Al₂O₃) ceramic ball for the total duration of 20 min, under dry sliding condition. Nanoindentation tests were also conducted using Berkovich nanoindenter for the purpose of measurement of hardness and elastic modulus values. However, the average value of friction coefficient (COF) corresponding to MCD and NCD coatings decrease from ~0.37–0.32 and ~0.30–0.27, respectively when the load is increased from 1–10 N. However, for conventional WC-Co substrate the average COF increases from ~0.60–0.75, under the same input operating conditions. The wear tracks formed on the surfaces of NCD, MCD and WC-Co, after sliding were characterised using Raman spectroscopy and scanning electron microscopy (SEM) techniques. Therefore, the results will serve breakthrough information for the designer to design the cutting tool or mechanical component using this novel coating procedure.

Corresponding author:

Kaleem Ahmad Najar
NIT Srinagar,
Kashmir, India.
E-mail: najar.kaleem@gmail.com

© 2017 Published by Faculty of Engineering

1. INTRODUCTION

Chemical vapor deposition (CVD) diamond coating has a combination of excellent mechanical and tribological properties, such as extremely high hardness, exceptional wear

resistance, and a low friction coefficient, sliding against a variety of counter bodies including ceramics and metals [1]. It has attracted great interests to be used as protective and wear-resistant film on mechanical bearings and seals in rotary

machines, such as pumps, turbines, compressors and hydraulic cylinders [2-4].

Cemented tungsten carbide (WC-Co) is the most commonly used tool material because of its high hardness as well as high elastic modulus and thus, diamond-coated WC-Co tools are mostly applicable for machining of non-ferrous metals, alloys, metal-matrix composite materials and hard brittle non-metals [5,6]. Since, the presence of cobalt binder (Co) content at surface of WC-Co substrate allows the formation of graphitic-carbon phases at the interface of coating-substrate system, thus decreases the adhesion of diamond films on WC-Co substrates [7]. Hence, an important technique to increase the quality of adhesion between coating and substrate is by the removal of surface cobalt, called chemical etching [8].

Since, the surface kinetics, vapor mass transport, thermodynamics of the system, chemistry of the reaction and processing parameters like temperature, pressure etc. are the main controlling parameters in CVD diamond process. During deposition process the growth rate of CVD diamond films is mainly controlled by the formation of required species to be deposited and its transportation in the vapor and surface kinetics [9]. The hot filament chemical vapour deposition (HFCVD) method is the most popular technique to achieve synthetic diamond coatings for machining and mechanical applications. HFCVD technique minimizes the price of synthetic diamond, because of its simplicity and comparatively low capital and operating cost [10].

Based on the diamond film grain size, coatings are mainly classified into nanocrystalline diamond (NCD) and microcrystalline diamond (MCD). However, the grain size of the diamond film is automatically controlled by methane concentration and chamber pressure during the deposition process [11]. By decreasing the grain size the internal stresses within a coating system increase and the presence of large number of grain boundaries in NCD layer is the source of graphitic-carbon phases, which decreases the crystallinity as well as the mechanical properties. Therefore, using an adhesive and smooth NCD film on WC-Co material is mostly suitable for tribological applications [12,13].

Thus, NCD films show low hardness, low elastic modulus, low friction coefficient and low adhesion (on ceramic substrates) in comparison to MCD films due to presence of non-diamond carbon at their grain boundaries [14].

While in machining of non-ferrous materials such as of Al-Si alloys, the polycrystalline diamond coated-tools (PCD) as well as nanocrystalline diamond (NCD) coated-hard metallic inserts were used most effectively [15]. However, the most important achievements in the last years in the area of improvement of ceramic cutting tools is the employment of hard anti-wear PVD-coatings deposited onto these ceramic tool inserts from the gaseous phase deposition method [16].

Typically, coatings used for tribological application are subjected to high load and sliding velocities, and therefore require sufficiently good adhesion, good surface finish and thermal stability in order to perform well. Generally, low friction materials usually possess friction coefficients below 0.1 in the presence of liquid lubrication, and from 0.3 down to 0.08 under boundary layer and dry friction conditions [17]. However, the adhesive failure event (coating de-lamination from the substrate) can be identified from the variation in the slope of the tangential force curve due to the change in the friction contact. For NCD coating, critical adhesive failure was observed at ~20 N under dynamic loading conditions. However, this adhesive failure event in MCD coating is observed at a much higher normal load of ~42 N. In this aspect, MCD coating exhibits superior scratch resistance due to its high hardness and crystallinity [18].

In the present work, the friction characteristics of WC-Co substrate and diamond coatings were compared, using ball-on-disc type linear reciprocating micro-tribometer, sliding against smooth Al₂O₃ ceramic counter ball, under dry sliding conditions. Also, the nanoindentation tests were carried out using Berkovich nanoindenter and the hardness values were calculated from the load-displacement data. In this research, it is expected to find the variations in COF on diamond-coated WC-Co substrates and uncoated-WC-Co substrate under the influence of increasing normal load, sliding time and nature of diamond film, which may significantly improve the performance of mechanical components in industry.

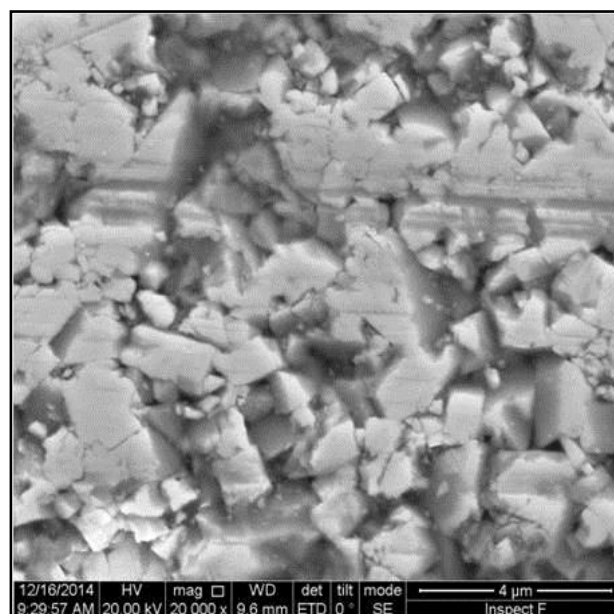
2. MATERIALS AND METHODS

Cemented tungsten carbide (WC-Co: CERATIZIT-CTF12A grade) with 6%Co and 0.8–1.3 μm WC grain size was selected as the substrate material in order to minimize the residual compressive stress developed during deposition process. WC-Co substrates of size 1×1×0.3 cm and with surface roughness factor (Ra) of $\sim 0.35 \mu\text{m}$ were cleaned in ethyl alcohol with ultrasonic agitation to remove the impurities from the surface. From these WC-Co samples, the surface cobalt was removed using standard chemical etching method to improve the strength of adhesion between coating and substrate. NCD and MCD coatings were deposited on two WC-Co substrates, using hot filament chemical vapour deposition (HFCVD) technique with uniform thickness of $\sim 3 \mu\text{m}$. Structural characteristics of the coatings were studied using grazing incidence X-ray diffraction technique (PANalytical) with $\text{CuK}\alpha$ ($\lambda=0.154 \text{ nm}$) radiation at 3° grazing angle and confocal Raman microscope technique (Alpha300R, WITec) at an excitation wavelength of 448 nm. Surface morphology of the coatings were studied using a high resolution scanning electron microscope (HRSEM, Quanta 3D, FEI). Cross-sections of these coatings were prepared using a precision low speed saw (ALLIED TechCut) with a resin bonded diamond wheel. Moreover, the topography of these coatings was studied using atomic force microscope (AFM, Dimension EDGE, Bruker). Antimony (n) doped silicon tip with nominal radius of curvature of $\sim 8 \text{ nm}$ was used and scanning was done in tapping mode. Nanoindentation tests were conducted using triboindenter (TI 950, HYSITRON) with a Berkovich tip of total included angle (2α) = 130.5° , radius of curvature approximately 150 nm and at 10 mN trapezoidal load cycle. The hardness values were calculated from the load-displacement data and the values of elastic modulus were calculated using Oliver and Pharr method. Friction characteristics were studied using a ball-on-disc type linear reciprocating micro-tribometer (CSM Instruments, Switzerland) under dry sliding conditions.

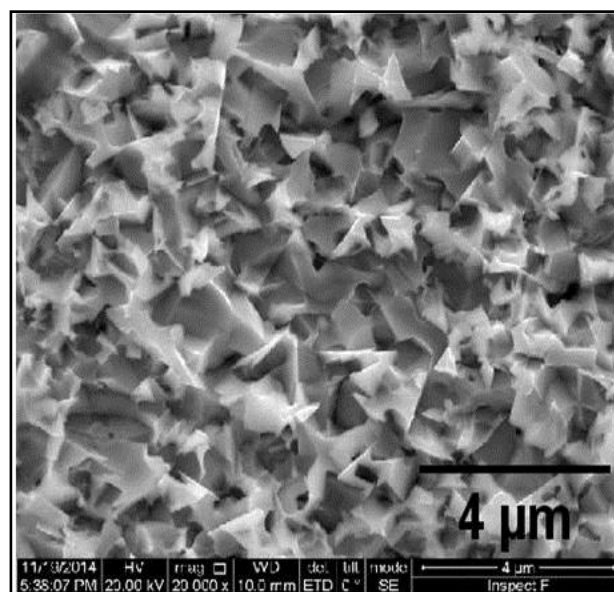
2.1. Chemical etching technique

Substrates were chemically treated with Murakami's reagent (10g KOH+10g $\text{K}_3[\text{Fe}(\text{CN})_6]$ +100 ml water) for 10 min using

ultrasonic agitation followed by cobalt etching for 10 sec with Caro's acid (3 ml (96 %) H_2SO_4 +88 ml (30 %) H_2O_2). Then the samples were seeded with nanodiamond particles (4–6 nm) in gel form for 10 min by ultrasonic agitation to increase the nucleation density. Samples were finally treated with isopropyl alcohol for 2 min to remove the loosely bound nanodiamond particles from the surface. Figure 1 (a, b, c) show the surface morphology of cemented tungsten carbide (WC-6%Co) before treatment, and after treatment from Murakami Reagent and Caro's acid, respectively. Surface cobalt was removed by Caro's acid and tungsten etching was done by Murakami Reagent to form cavities on the surface in order to increase the strength of adhesion.



a)



b)

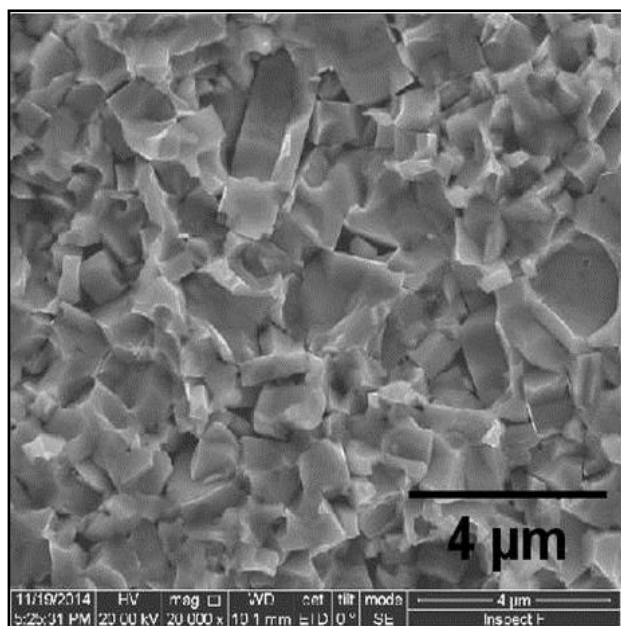


Fig. 1. Surface morphology of WC-Co sample (a) Before treatment, and after treatment from, (b) Murakami Reagent and (c) Caro's acid.

2.2. Method of deposition

Hot filament chemical vapor deposition system (HFCVD, Model 650 series, sp³ Diamond Technologies) with excellent process control unit system was used for the deposition of diamond films, using growth rate of 1 μm/hr. Deposition parameters such as chamber pressure and methane concentration were controlled easily during the experiment by using throttle valve and mass flow controllers, respectively. Hydrogen (H₂) and methane (CH₄) were used as the precursor gases and their flow rates were completely controlled using mass flow controllers. An array of tungsten wires (∅ 0.12 mm) in systematic order were used as hot filaments for the activation of these precursor gases and the distance between filament and substrate was kept 15 mm. The grain size of the diamond films were usually controlled by both methane concentration and chamber pressure. Thus, the growth parameters used for the deposition of MCD and NCD coatings are listed in Table 1. The exhaust gases produced after the deposition process from the HFCVD chamber were diluted using nitrogen (N₂) gas. N₂ gases were used before and after the diamond growth process to flush the chamber. CVD-chamber was made of aluminum with cooling channels and the temperature of the chamber was maintained at ~50 °C using a circulating water chiller. Figure 2 (a, b, c) show the picture of HFCVD

instrument, inside view of the chamber and view of the hot filaments over flat substrates during diamond nucleation process, respectively.

Table 1. Growth parameters used for the deposition of MCD & NCD coatings.

Coating Type	Process Pressure (Torr)	CH ₄ /H ₂ Conc. (%)	Filament Temp. (°C)	Substrate Temp. (°C)	Duration (hrs)
MCD	36	2	~2200	~800	3
NCD	12	4	~2200	~800	3

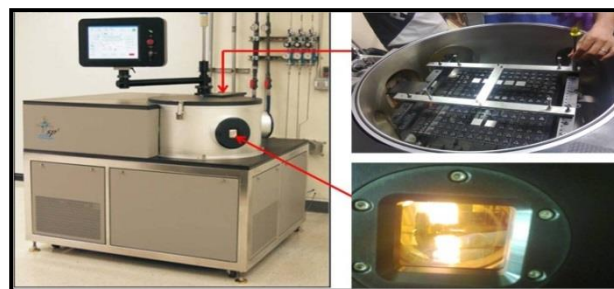


Fig. 2. (a) HFCVD instrument, (b) Inside view of the chamber and (c) View of the hot filaments over WC-Co substrates during diamond growth.

2.3 Experimental procedure

NCD and MCD coatings (each ~3 μm thick) have been achieved successfully for three hours on chemically etched cemented tungsten carbide substrates, using HFCVD technique by controlling the process parameters. In the present work, nanoindentation tests were carried out using Berkovich nanoindenter and their values were calculated from the load-displacement data. The friction characteristics of uncoated WC-Co substrate and diamond-coated WC-Co substrates were compared, using ball-on-disc type linear reciprocating micro-tribometer. Experiments were conducted at normal loads 1, 5 and 10 N, sliding velocity 8cm/s, stroke length 5 mm, frequency 2 Hz, temperature 30±1 °C, sliding time 20 min and relative humidity ~60 %, under dry sliding test conditions. Alumina (Al₂O₃) ball of size 6 mm was used as sliding body under the application of increased load condition. Hence, the detailed experimental conditions are listed in Table 2.

However, during tribological study the fundamental parameters like normal load, sliding velocity, surface roughness, coating type, atmospheric condition, sliding time, counter ball material, stroke and frequency were selected for the measurement of variation in friction

coefficient. Therefore, the lower load conditions (minimum basic fundamental load) with increasing magnitude were chosen in order to compare the effect on the friction and wear characteristics on diamond-coated WC-Co samples with uncoated one, after sliding against Al₂O₃ ceramic ball.

Table 2. Experimental conditions.

S. No.	Parameters	Operating Conditions
1	Normal Load	1, 5, 10 N
2	Sliding Velocity	8 cm/s
3	Relative Humidity	60 (± 5)%
4	Duration of Rubbing	20 minutes
5	Surface Condition	Dry
6	Materials Tested	WC-Co, MCD & NCD
7	Ball Material	Al ₂ O ₃
8	Diameter of ball	6 mm
9	Stroke length	5 mm
10	Frequency	2 Hz
11	Temperature	30 ± 1 °C
12	Roughness Factor (Ra): WC-Co MCD NCD	 ~0.35 μ m ~0.28 μ m ~0.19 μ m

3. RESULTS AND DISCUSSIONS

3.1 X-ray diffraction patterns of MCD and NCD coatings

The XRD patterns of MCD and NCD coatings are shown in Fig. 3 (a, b) respectively, sharp and strong peaks of cubic diamond coatings were observed at (111) crystal and (220) crystal planes at diffraction angles of 44° and 75.5° respectively for both coatings, along with the tungsten carbide (WC) peaks.

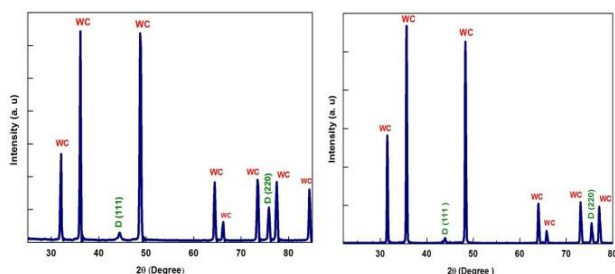


Fig. 3. X-ray diffraction patterns of (a) MCD coating and (b) NCD coating.

These observed peaks confirm the crystallinity of both the coatings [18]. The diamond peaks of MCD coating appears slightly higher than that of

NCD coating, which clearly confirm that the grain sizes are different. The highest peaks of WC substrate show that its grain size is more than diamond coatings.

3.2 Raman spectroscopy of MCD and NCD coatings

Raman spectroscopy was used to check the nature and crystallinity of the diamond coatings and if the crystalline diamond coating shows a fundamental Raman peak at approximately 1333 cm⁻¹, confirms that the coating is diamond in nature [19]. Figure 4 (a, b) show the Raman spectra of MCD and NCD coatings respectively. The shift of this fundamental Raman peak towards higher value confirms the presence of residual compressive stresses in both types of coatings. The presence of these residual compressive stresses in diamond coatings are mainly due to the difference of thermal expansion coefficients between the coating and substrate [20]. Hence, these residual stresses are calculated from $\sigma = -0.348 (v_m - v_0)$ GPa for the fundamental Raman peak at v_m , where $v_m = 1334$ cm⁻¹ and $v_0 = 1333$ cm⁻¹ [21]. Therefore, each deposited diamond film contains residual stresses of -0.348 GPa, where negative sign indicates compressive stress. The presence of two other peaks v_1 and v_3 are properties of in-plane (C-H) and stretching (C=C) vibrational modes respectively, and these modes were ascribed to the formation of transpoyacetylene chain in the grain boundaries which is a common behaviour of NCD coatings [22]. Also, the other peak (G-band) as shown on the right side of fundamental Raman peak indicates the presence of graphitic carbon phases at the grain boundaries of NCD coating.

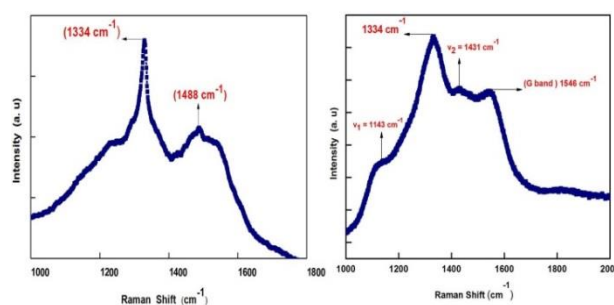
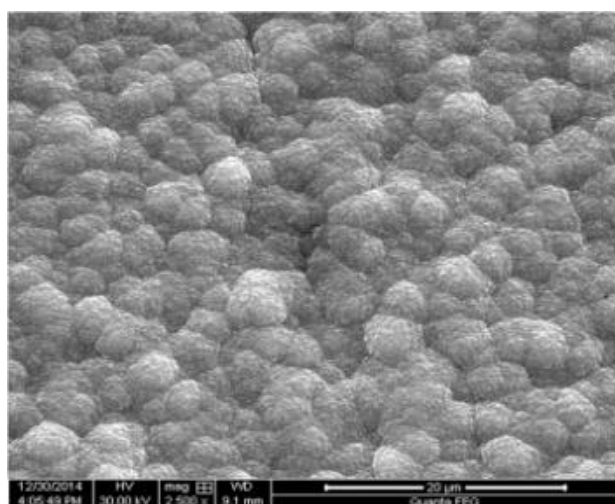


Fig. 4. Raman spectra of (a) MCD coating and (b) NCD coating.

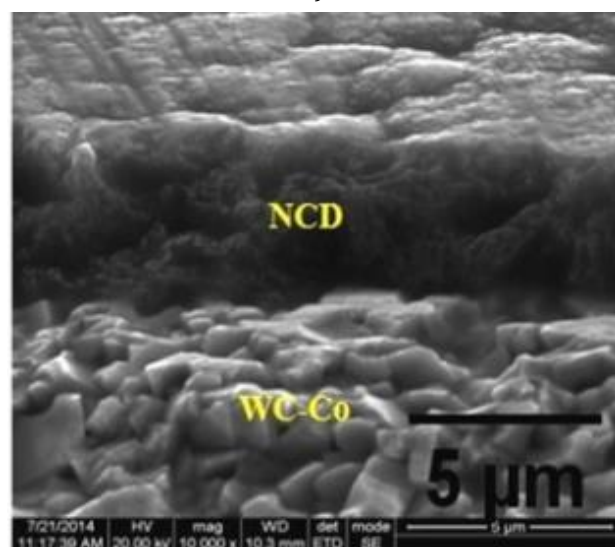
3.3 Surface topography of MCD and NCD coatings

Scanning electron microscopy (SEM) technique was used to study the surface morphology,

microstructure and grain size of nano-diamond coatings. Since during diamond growth process increasing methane concentration affects the crystalline quality and generally above 4 % the nanocrystalline grains are formed. Hence, increase in methane concentration gives secondary diamond nucleation and therefore, a cauliflower type of grain shape is mainly observed at the NCD surface. In case of MCD coating the columnar structure of grains and faceted form of surface morphology was generally observed at methane concentration of 1 % [23]. Figure 5 (a, b) and Fig. 6 (a, b) show the typical surface morphology and cross-sectional view of the NCD and MCD coatings, respectively. However, the compositional elemental analysis on the surfaces of both coatings was confirmed using energy dispersive spectroscopy (EDS) technique, as shown in Fig. 7.

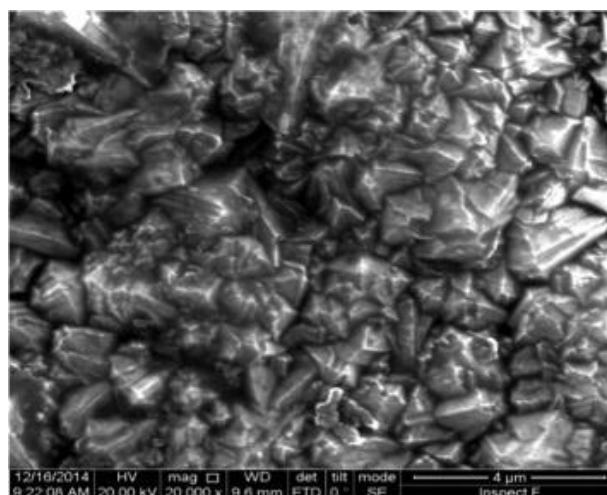


a)

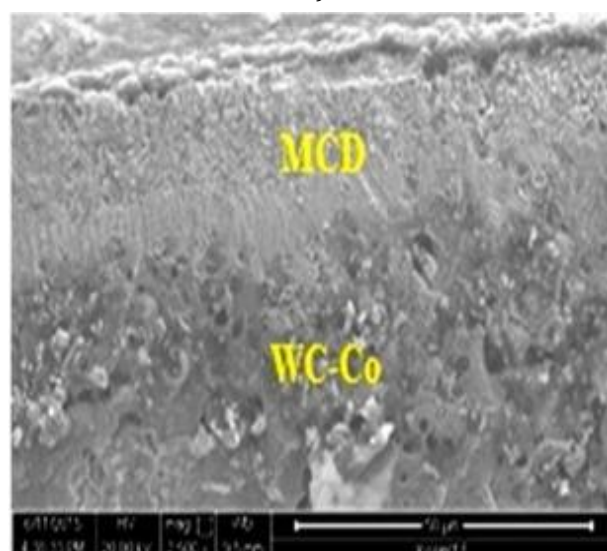


b)

Fig. 5. (a) Surface morphology of NCD coating and (b) Cross-sectional morphology of NCD coating.



a)



b)

Fig. 6. (a) Surface morphology of MCD coating and (b) Cross-sectional morphology of MCD coating.

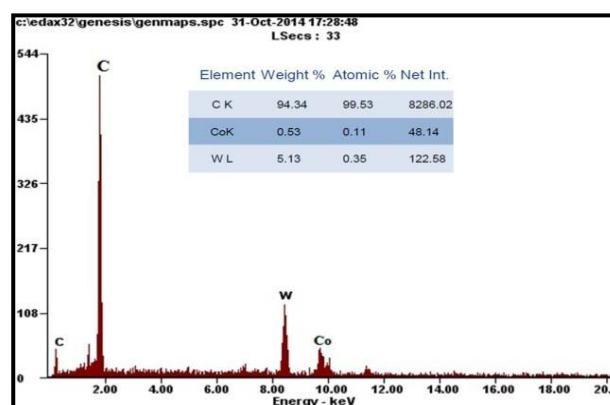


Fig. 7. Energy dispersive spectroscopy (EDS) analysis on the surfaces of NCD and MCD coatings.

Furthermore, the AFM imaging was carried out in tapping mode and gives the complete technical details of height imaging. AFM height image gives better topographical contrast and

details in comparison to HRSEM image. Here the NCD and MCD coatings show different AFM images with different height parameters as shown in Fig. 8 (a, b), respectively. During this AFM technique similar areas of the NCD and MCD coatings were scanned as in SEM technique and presented here. Fig.8 (a) shows the 2D-AFM image of the NCD coating at a scanning area of $2 \times 2 \mu\text{m}^2$. Small grain sizes with cauliflower type of smooth structures were observed on the NCD surface and thus possess good tribological properties. Also, the height details of these features were represented as a color scale on the AFM height image and listed in Fig. 8. Similarly, same area of the MCD coating was also scanned using AFM and presented here. Fig. 8 (b) shows the AFM height image of the MCD coating at scanning area of $2 \times 2 \mu\text{m}^2$. Large grain sizes with faceted type of smooth structures were observed on the MCD surface, but the sharp features that observed on the MCD surface were unfavorable to their use for tribological applications.

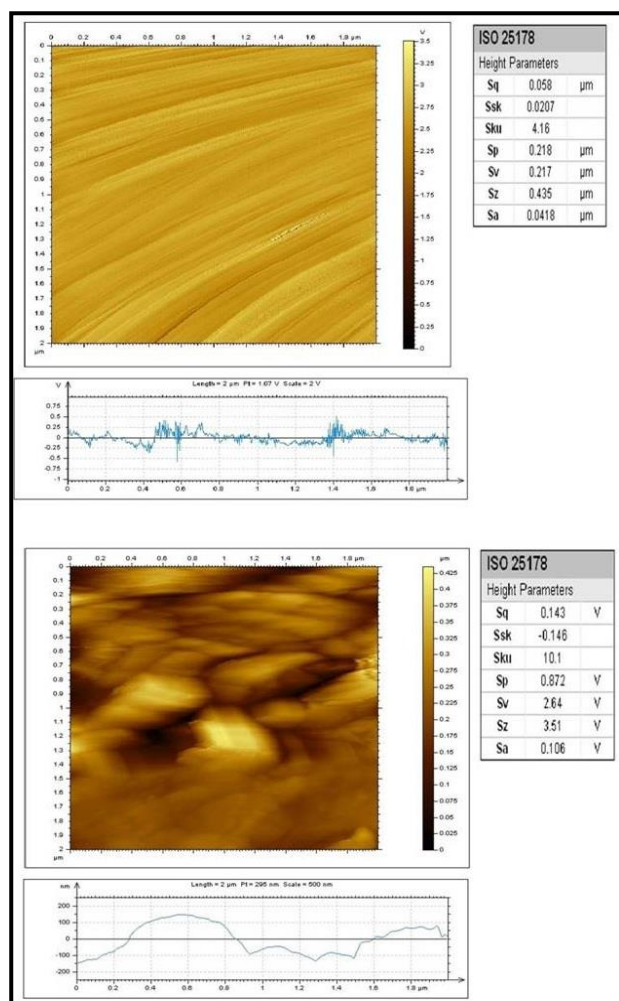


Fig. 8. AFM height image ($2 \times 2 \mu\text{m}^2$) of (a) NCD coating and (b) MCD coating.

3.4 Nanoindentation and hardness measurement of MCD and NCD coatings

Before nanoindentation tests the MCD and NCD coatings were polished against Si_3N_4 pin for the duration of 2hrs using a tribometer. Figure 9 (a, b) show the load-displacement curves for the polished MCD and NCD coatings, respectively. Three indentation tests were carried out on each coating using Berkovich nanoindenter. The average indentation depths for MCD and NCD coatings were found 65nm and 73 nm and their excellent average hardness values were ~ 50 GPa and ~ 40 GPa, respectively. Also, the elastic modulus values of MCD and NCD coatings were ~ 1100 GPa and ~ 1000 GPa respectively, as calculated mathematically from Oliver and Pharr method [24] as:

$$\text{Hardness (H)} = P/A = P / 24.5 h_c^2 \text{ and Stiffness (S)} = dP/dh = 2E^*(\sqrt{A}/\sqrt{P}) \quad (1)$$

$$\text{Elastic modulus (E)} = (\text{slope of the elastic unloading curve}) \times (\sqrt{\pi}/2\sqrt{A}) \quad (2)$$

$$\text{Reduced modulus, } 1/E^* = 1-\nu^2/E + 1-\nu^2/\dot{E} \quad (3)$$

$$E^* = dP/dh (1/2h_c) (1/\beta) [\sqrt{\pi}/24.5] \quad (4)$$

$$A = 3 (\sqrt{3} h_c^2) \text{Tan}^2 (65.3) = 24.5 h_c^2 \text{ and } \beta = 1.034 \text{ for Berkovich indenter} \quad (5)$$

where, P=maximum load, A=area of contact, h_c is the contact depth, E=elastic modulus of specimen and \dot{E} =elastic modulus of indenter.

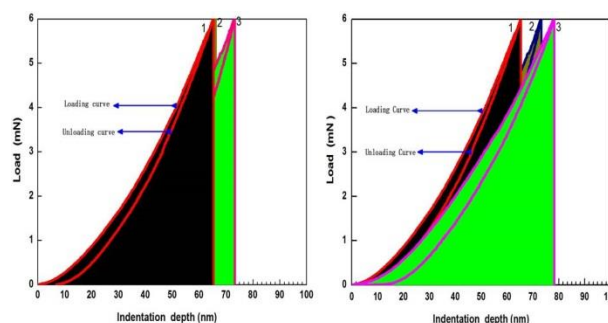


Fig. 9. Load-displacement curves corresponding to 3 indentations on (a) MCD coating and (b) NCD coating.

3.5 Friction characteristics of WC-Co and CVD-diamond coatings

Frictional characteristics of the CVD-diamond coatings and WC-Co substrate were compared using ball on disc-Micro-tribometer, sliding against smooth alumina (Al_2O_3) ceramic ball, under the application of increased normal load.

However, the average COF corresponding to NCD coating decreases from ~ 0.30 – 0.27 by increasing the load from 1–10 N, for the total duration of 20 min, as shown in Fig. 10 (a). Similarly, the average COF for MCD coating decreases from ~ 0.37 – 0.32 , under the same input operating conditions, as shown in Fig. 11 (a). Figure 10 (b, c, d) show the HRSEM images of the wear tracks corresponding to NCD coating at 1 N, 5 N and 10 N load respectively, with the formation of tribo-layer. Similarly, Fig. 11 (b, c, d) show the HRSEM images of the wear tracks corresponding to MCD coating at 1 N, 5 N and 10 N load respectively, with the formation of tribo-layer.

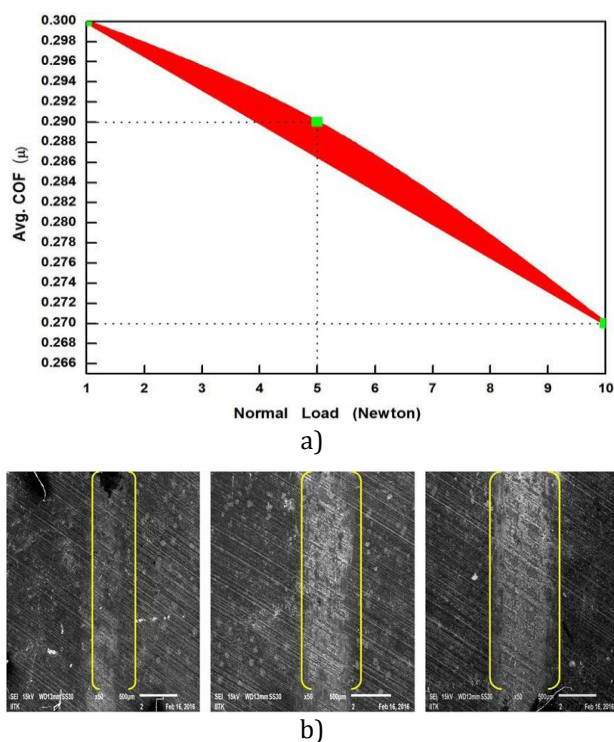


Fig. 10. NCD coating, sliding against Al_2O_3 ball using ball on disc-Micro-tribometer (a) Variation of COF with respect to normal load, and (b, c, d) Wear-track morphology at 1 N, 5 N and 10 N load.

This can be clearly observed from all the wear-tracks that with the increase in magnitude of load the track-width increases and also the surface roughness decreases, and therefore corresponding COF decreases on the surfaces of each coating. However, all CVD-diamond coatings undergo phase transformation during long-duration of rubbing, high-load (high-speed) sliding tests, and then the transformation products trapped at the sliding interfaces can periodically influence the friction and wear performance [25]. This observed low hardness, high indentation depth and low COF of NCD

coating in comparison to that of MCD coating were observed due to the presence of graphitic-carbon phases at the grain boundaries, and also due to its small grain size. However, the observed initial higher value of COF in case of MCD coating is mainly due to high surface roughness and it becomes lower with sliding, and shows COF comparable to that of NCD coating.

Generally the COF regarding uncoated-WC-Co surface increases from ~ 0.60 – 0.75 by increasing the normal load from 1–10 N, as shown in Fig. 12 (a). Figure 12 (b, c, d) show the HRSEM images of the wear-tracks corresponding to WC-Co substrate at 1 N, 5 N and 10 N load, respectively. Since, little changes are observed on the wear-tracks of uncoated-WC-Co surface at each load but, the surface roughness increases with the increase in magnitude of load. Therefore, the corresponding values of COF increase with increasing normal load and this is in accordance with law of mechanics as: $F = \mu R$.

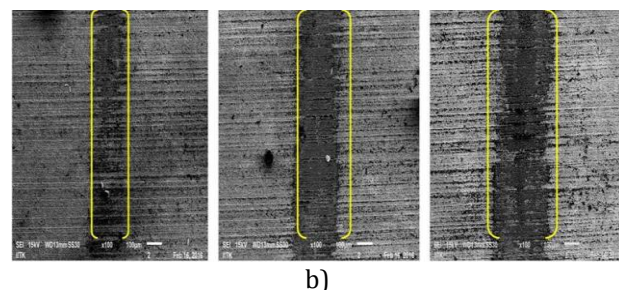
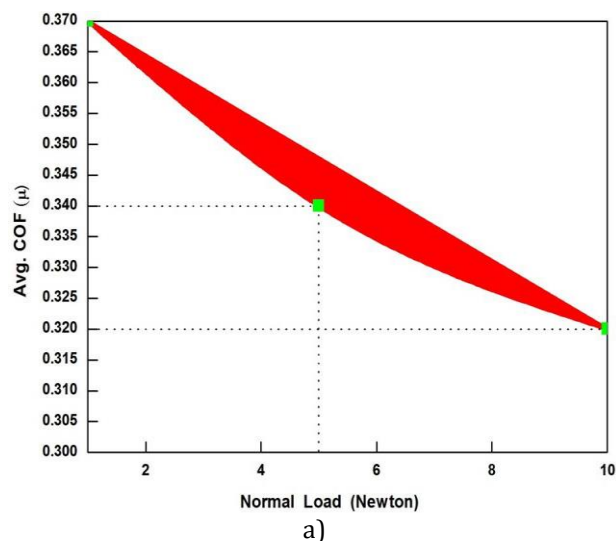


Fig. 11. MCD coating, sliding against Al_2O_3 ball using ball on disc-Micro-tribometer (a) Variation of COF with respect to normal load, and (b, c, d) Wear-track morphology at 1 N, 5 N and 10 N load.

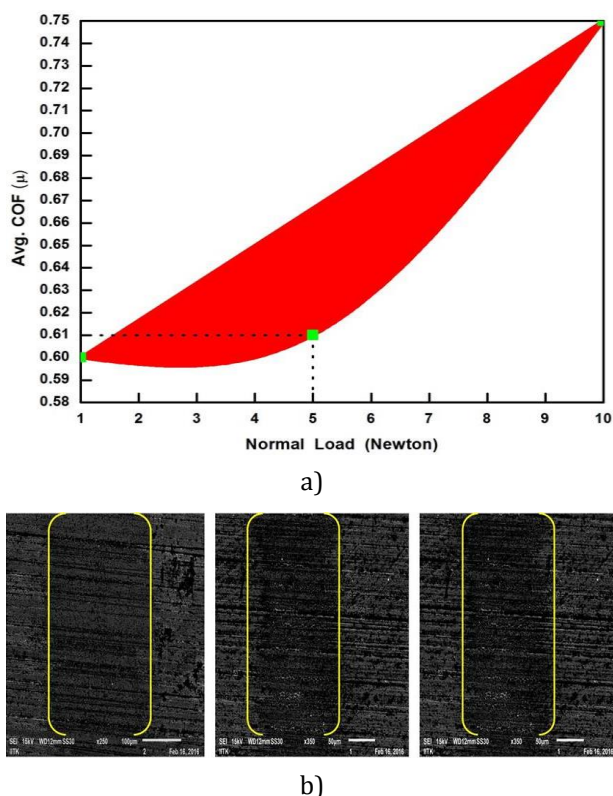


Fig. 12. WC-Co substrate, sliding against Al₂O₃ ball using ball on disc-Micro-tribometer (a) Variation of COF with respect to normal load, and (b, c, d) Wear-track morphology at 1 N, 5 N and 10 N load.

Table 3. Mechanical and tribological results.

Material Type	Indentation Depth (h)	Hardness (H)	Elastic Modulus (E)	Variation in COF (μ)
MCD	~65 nm	~50 GPa	~1100 GPa	~0.37-0.32
NCD	~73 nm	~40 GPa	~1000 GPa	~0.30-0.27
WC-Co		~18 GPa	~550 GPa	~0.60-0.75

However, the reverse process occurred on the surfaces of all CVD-diamond coatings during friction testing i.e. the COF increases with increasing load. Therefore, the friction coefficient and wear resistance can be maintained, by maintaining the appropriate level of sliding speed and normal load to improve mechanical processes [26]. Thus, the detailed mechanical and tribological experimental results are summarized in Table 3.

3.6 Raman spectra of NCD and MCD wear-tracks

Figure 13 (a, b, c) show the Raman spectra of wear-tracks corresponding to NCD coating at 1 N, 5 N and 10 N loads respectively, sliding against Al₂O₃ ball after friction measurement. Similarly, Fig. 14 (a, b, c) show the Raman

spectra of wear-tracks corresponding to MCD coating at 1 N, 5 N and 10 N loads respectively, under the same input experimental conditions. Generally, the presence of residual compressive stresses in NCD and MCD wear-tracks are also calculated from $\sigma = -0.348 (v_m - v_0)$ GPa for the fundamental Raman peak at $v_m = 1340 \text{ cm}^{-1}$ and $v_0 = 1333 \text{ cm}^{-1}$. Therefore, each wear-track of both diamond coatings contains residual compressive stresses of 2.436 GPa, under the application of each load. Thus, after friction measurement the residual compressive stresses corresponding to the wear-tracks of both diamond coatings increases, but the magnitude remained same with the increase in load. The variations of two other peaks (v_1 and v_3) on both sides of the fundamental diamond peak (1340 cm^{-1}) at each load for both diamond coatings, represent the change in-plane (C-H) and stretching (C=C) vibrational modes respectively, which occurred due to the application of increased load.

Furthermore, Fig. 15 (a) shows surface morphology of the Al₂O₃ counter ball and Fig.15 (b) shows elemental compositional analysis of the tribo-layer (tribo-oxide) formed on the wear-tracks of each diamond coating after sliding against Al₂O₃ ball material, using energy dispersive spectroscopy (EDS) technique. Since, aluminum particles were transferred from the Al₂O₃ ball material onto the wear-tracks of NCD and MCD coatings after sliding, as confirmed from the EDS diagram, where Al peak is present. Thus, the adhesive type of wear exists in this work.

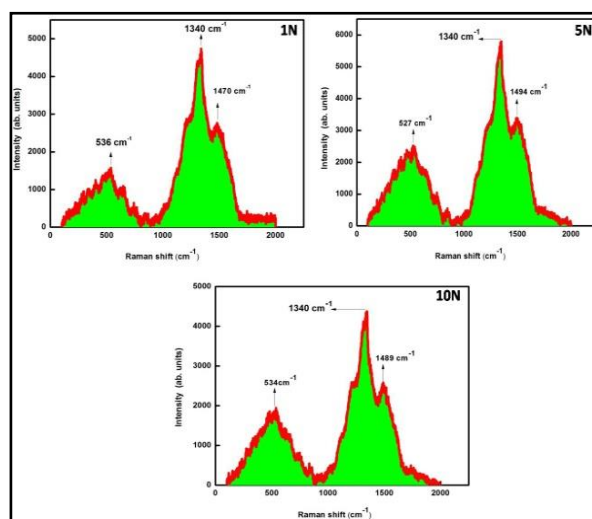


Fig. 13. Raman spectra of the NCD wear-tracks obtained after friction measurement, sliding against Al₂O₃ ball at (a) 1 N, (b) 5 N and (c) 10 N load.

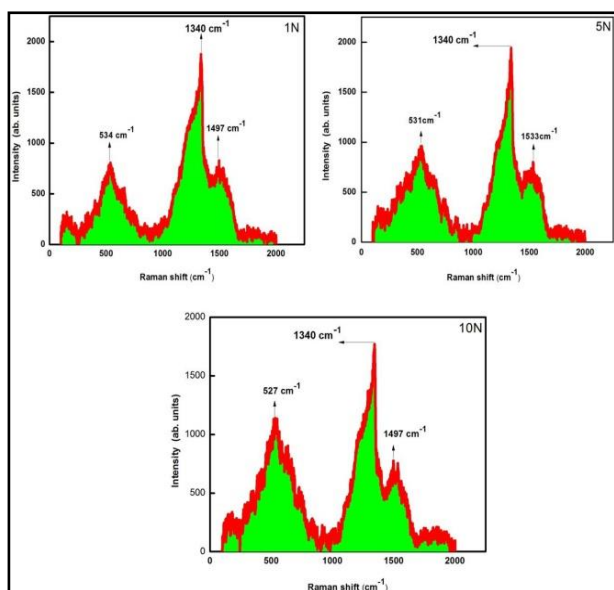


Fig. 14. Raman spectra of the MCD wear-tracks obtained after friction measurement, sliding against Al_2O_3 ball at (a) 1 N, (b) 5 N and (c) 10 N load.

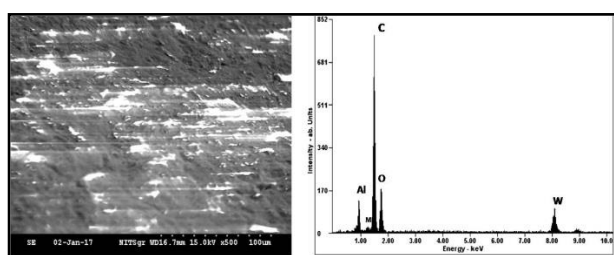


Fig.15. (a) Surface morphology of Al_2O_3 counter ball after sliding against diamond coatings and (b) EDS analysis of the tribo-layer formed on the MCD and NCD wear-tracks.

CONCLUSION

The obtained results reveal that the COF of diamond coated-WC-Co substrate decreases with the increase in magnitude of load. Here, the NCD coating has shown the lowest value of COF; however MCD coating has shown the higher value of COF initially, but becomes comparable to that of NCD coating after 20 min of sliding time. Thus, taking into consideration the hardness and frictional characteristics of CVD-diamond coatings, the MCD coating is found good for load-bearing industrial applications due to its high hardness as well as high elastic modulus; however, the NCD coating increases only tribological properties of the WC-Co substrate. The residual compressive stresses also increase with the increase in load during friction measurement, as confirmed from Raman spectroscopy technique. Therefore, maintaining

an appropriate level of normal load and appropriate type of diamond coating, friction may be kept to some lower value to improve mechanical processes.

Acknowledgement

The Authors would like to thank to MSRC lab, IIT Madras for the deposition of diamond coatings and Surface Engineering Division, NAL, Bangalore, India for doing tribological tests. One of the Author, Mr. Kaleem Ahmed Najar is very thankful to Shoib Mushtaq (Mech. Dept, NIT Srinagar), Jibran Khan (Mech. Dept, NIT Srinagar), Farooq Ahmad Dar (Physics Dept, NIT Srinagar) and Ashaq Hussain Sofi (Physics Dept, NIT Srinagar) for their good assistance during my experimental work.

REFERENCES

- [1] X. Lei, B. Shen, S. Chen, L. Wang and F. Sun, 'Tribological behavior between micro- and nanocrystalline diamond films under dry sliding and water lubrication', *Tribology International*, vol. 69, pp. 118–127, 2014.
- [2] A. Sumant, A. Krauss, D. Gruen, O. Auciello, A. Erdemir and M. Williams, 'Ultranano-crystalline Diamond Film as a Wear-Resistant and Protective Coating for Mechanical Seal Applications', *Tribology Transactions*, vol. 48, pp. 24–31, 2005.
- [3] P. Hollman, H. Björkman, A. Alahelisten and S. Hogmark, 'Diamond coatings applied to mechanical face seals', *Surface and Coatings Technology*, vol. 105, pp. 169–174, 1998.
- [4] M. Perle, C. Bareiss, S. Rosiwal and R. Singer, 'Generation and oxidation of wear debris in dry running tests of diamond coated SiC bearings', *Diamond and Related Materials*, vol. 15, pp. 749–753, 2006.
- [5] A. Inspektor, E.J. Oles and C.E. Bauer, 'Theory and practice in diamond coated metal-cutting tools', *International Journal of Refractory Metals and Hard Materials*, vol. 15, pp. 49–56, 1997.
- [6] F.H. Sun, Z.M. Zhang, M. Chen and H.S. Shen, 'Improvement of adhesive strength and surface roughness of diamond films on Co-cemented tungsten carbide tools', *Diamond and Related Materials*, vol. 12, pp. 711–718, 2003.
- [7] B. Shen and F. Sun, 'Deposition and friction properties of ultra-smooth composite diamond

- films on Co-cemented tungsten carbide substrates, *Diamond and Related Materials*, vol. 18, pp.238-243, 2009.
- [8] Z. Xu, L. Lev, M. Lukitsch and A. Kumar, 'Effects of surface pretreatments on the deposition of adherent diamond coatings on cemented tungsten carbide substrates', *Diamond and Related Materials*, vol. 16, pp. 461–466, 2007.
- [9] M.A. Chowdhury and D.M. Nuruzzaman, 'Influence of Gas Flow Rate on the Deposition Rate on Stainless Steel 202 Substrates', *Tribology in Industry*, Vol. 34, pp. 226–231, 2012.
- [10] D. Zhang, B. Shen and F. Sun, 'Study on tribological behavior and cutting performance of CVD diamond and DLC films on Co-cemented tungsten carbide substrates', *Applied Surface Science*, Vol. 256, pp. 2479–2489, 2010.
- [11] M. Ali and M. Ürgen, 'Surface morphology, growth rate and quality of diamond films synthesized in hot filament CVD system under various methane concentrations', *Applied Surface Science*, vol. 257, pp. 8420–8426, 2011.
- [12] D. Schwarzbach, R. Haubner and B. Lux, 'Internal stresses in CVD-diamond layers', *Diamond and Related Materials*, vol. 3, pp. 757–764, 1994.
- [13] M. Wiora, K. Brühne, A. Flöter, P. Gluche, T. M. Willey, S. O. Kucheyev, A. W. Van Buuren, A. V. Hamza, J. Biener and H.-J. Fecht, 'Grain size dependent mechanical properties of nanocrystalline diamond films grown by hot-filament CVD', *Diamond and Related Materials*, vol. 18, pp. 927–930, 2009.
- [14] R. Dumpala, M. Chandran, N. Kumar, S. Dash, B. Ramamoorthy and M.S. Ramachandra Rao, 'Growth and characterization of integrated nano- and microcrystalline dual layer composite diamond coatings on WC-Co substrates', *International Journal of Refractory Metals and Hard Materials*, vol. 37, pp. 127-133, 2013.
- [15] K.-D. Bouzakis, G. Skordaris, E. Bouzakis, D. Tasoulas, P. Charalampous, T. Kotsanis, S. Kombogiannis and O. Lemmer, 'Explanation of the Wear Behaviour of NCD Coated Carbide Tools Facilitated by Appropriate Methods for Assessing the Coating Adhesion Deterioration at Elevated Temperatures', *Tribology in Industry*, Vol. 37, pp. 309–319, 2015.
- [16] M. Sokovic, J. Kopac, L. A. Dobrzanski, J. Mikula, K. Golombek and D. Pakula, 'Cutting Characteristics of PVD and CVD - Coated Ceramic Tool Inserts', *Tribology in industry*, Vol. 28, pp. 3–8, 2006.
- [17] A. Koutsomichalis, N. Vaxevanidis, G. Petropoulos, E. Xatzaki, A. Mourlas and S. Antoniou, 'Tribological Coatings for Aerospace Applications and the Case of WC-Co Plasma Spray Coatings', *Tribology in industry*, Vol. 31, pp. 37-42, 2009.
- [18] R. Dumpala, N. Kumar, C.R. Kumaran, S. Dash, B. Ramamoorthy and M.S. Ramachandra Rao. 'Adhesion characteristics of nano- and microcrystalline diamond coatings: Raman stress mapping of the scratch tracks', *Diamond and Related Materials*, vol. 44, pp. 71-77, 2014.
- [19] S. Praver and R.J. Nemanich, 'Raman spectroscopy of diamond and doped diamond', *Philos. Trans. R. Soc. Lond., A*, vol. 362, pp. 2537–2565, 2004.
- [20] J. Gunnars and A. Alahelisten, 'Thermal stresses in diamond coatings and their influence on coating wear and failure', *Surface and Coatings Technology*, vol. 80, pp. 303–312, 1996.
- [21] M. Chandran, C.R. Kumaran, S. Gowthama, P. Shanmugam, R. Natarajan, S.S. Bhattacharya and M.S. Ramachandra Rao, 'Chemical vapor deposition of diamond coatings on tungsten carbide (WC-Co) riveting inserts', *International Journal of Refractory Metals and Hard Materials*, vol. 37, pp. 117–120, 2013.
- [22] H. Kuzmany, R. Pfeiffer, N. Salk and B. Günther, 'The mystery of the 1140cm⁻¹ Raman line in nanocrystalline diamond films', *Carbon*, vol. 42, pp. 911–917, 2004.
- [23] W. Kulisch and C. Popov, 'On the growth mechanisms of nanocrystalline diamond films', *Physics Status Solidification A*, vol. 203, pp. 203–219, 2006.
- [24] W.C. Oliver and G.M. Pharr, 'Improved technique for determining hardness and elastic modulus using load and displacement sensing indentation experiments', *Journal of Materials Research*, vol. 7, pp. 1564–1583, 1992.
- [25] A. Erdemir, G.R. Fenske, A.R. Krauss, D.M. Gruen, T. McCauley and R.T. Csencsits, 'Tribological properties of nanocrystalline diamond films', *Surface and Coatings Technology*, vol. 120, pp. 565–572, 1999.
- [26] M.A. Chowdhury, M.K. Khalil, D.M. Nuruzzaman and M.L. Rahaman, 'The Effect of Sliding Speed and Normal Load on Friction and Wear Property of Aluminum', *International Journal of Mechanical & Mechatronics Engineering*, vol. 11, pp. 111701–116868, 2011.